J Mater Sci (2007) 42:3066–3072
DOI 10.1007/s10853-006-0561-2

Erosion of geopolymers made from industrial waste

K. C. Goretta · F. Gutierrez-Mora · D. Singh · J. L. Routbort · G. C. Lukey · J. S. J. van Deventer

Received: 5 November 2006 / Accepted: 20 December 2006 / Published online: 14 April 2007

Abstract Solid-particle erosion studies were conducted on geopolymers derived from various combinations of granulated blast-furnace slag, flyash, sand, clay, and rock. The erodent particles were 390-μm angular Al_2O_3, which impacted at 30, 60, or 90° at a velocity of 50, 70, or 100 m/s. Steady-state erosion rates were obtained as weight of target lost per weight of impacting particles. Material-loss mechanisms were studied by scanning electron microscopy (SEM). All of the geopolymers responded to normal impact as conventional brittle solids, but impact at 30° led to anomalously rapid erosion, probably because of presence of microcracks and consequent enhanced removal of aggregates within the geopolymers. Erosion rates at 90° impact were proportional to erodent velocity to the 2.3–2.7 power. The geopolymers exhibited crushing strengths of approximately 32–57 MPa. Erosion rate correlated with density and strength for geopolymers of similar composition. All of the geopolymers that contained flyash were more resistant to erosion than was the geopolymer without flyash.

K. C. Goretta · F. Gutierrez-Mora · D. Singh · J. L. Routbort (✉)
Argonne National Laboratory, Argonne, IL 60439-4838, USA
e-mail: routbort@anl.gov

Present Address:
K. C. Goretta
AOARD, Tokyo 106-0032, Japan

Present Address:
F. Gutierrez-Mora
Department of Condensed Matter Physics, University of Sevilla, Sevilla, Spain

G. C. Lukey · J. S. J. van Deventer
Department of Chemical Engineering, The University of Melbourne, Melbourne, Victoria 3010, Australia

Introduction

Geopolymers are formed by condensation polymerization of alkali-activated aluminosilicates [1–13]. Synthesis of geopolymers from pure materials has been studied for decades [1–4], and much recent work on synthesis of geopolymers has focused on synthesis from waste products such as flyash and slag [4–13]. Although differing opinions exist as to the exact mechanism for geopolymeric reactions, it is apparent that often when waste materials are used as precursors that dissolution of the starting materials is incomplete when the final hardened structures are formed [7], and that a surface reaction is responsible for bonding the undissolved waste particles into the final geopolymer structure [8].

In contrast to currently used cement-based materials [14–19], comparatively little work has been conducted on the tribological properties and durability of geopolymers. For example, abrasion, water-erosion, and solid-particle-erosion studies have been conducted on various Portland and phosphate cements [14, 15, 20, 21]. Although we have also subjected a geopolymer based on blast-furnace slag and flyash to solid-particle erosion, only one composition has been studied [22, 23]. We found that it eroded rapidly, which led to the obvious question as to the effect of composition on erosion rate. In this work, we have eroded geopolymers that contain various combinations of blast-furnace slag, flyash, sand, clay, and coarse basalt aggregate. Erosion rates have been determined and mechanisms of materials removal have been identified.

Experimental procedures

Specimen preparation

Granulated blast-furnace slag, Class C flyash, sand, clay, and sodium/potassium silicate were used as starting materials. For one specimen, coarse basalt rock was added to achieve ≈25 vol.% of rock in the final composite (Table 1). All materials were weighed, placed into plastic containers, stirred for ≈300 s, and cast into 50-mm-diameter cylinders having a 1:2 diameter-to-length ratio. Each casting was vibrated for 2 min to minimize entrapment of air, and then cured at 315 K and 95% relative humidity. The castings were removed from the molds after 18 h, placed into sealed plastic bags, and stored at ambient temperature until needed for testing.

Characterization

Densities were determined geometrically. Compressive strengths, per Australian Standard 1012.9 [24], of the 50-mm-diameter specimens were measured with an Amsler FM 2750 testing apparatus. Three cylinders of each composition were tested and the experimental values were averaged. Samples were tested after curing for 28 days.

Microstructures were examined by optical and scanning electron microscopy (SEM). SEM specimens were coated with carbon and examined with a Hitachi S-4700-II microscope (Tokyo, Japan).

Erosion tests

Specimens for erosion testing were cut from the castings with a diamond-bladed saw. No surfaces were polished. Smaller specimens for study of individual impact sites were polished with 1-μm diamond paste [23]. Solid-particle erosion tests were carried out in a slinger-type apparatus that has been described previously [Ref. 25 and references therein]. Tests were conducted in vacuum (≈500 mTorr) and thus aerodynamic effects were negligible. The feed rate of the erodent, ≈0.13 g/s, was sufficiently low that interactions between erodent particles were negligible.

The erodent particles were angular Al_2O_3 abrasives (Alundum 38, Norton, Worcester, MA, USA) with mean diameter of ≈390 μm [20–23]. The angle of impact was 30, 60, or 90° and particle velocity (V) was 50, 70, or 100 m/s. All eroded surfaces were approximately 19 mm × 19 mm. Steady-state erosion rates (ERs, in mg/g) were determined from plots of specimen weight loss versus dose (weight of particles impacting the surface). At least four test runs were conducted for each specimen. Spent erodent was captured and also examined by SEM.

After the first erosion run, it became clear that the specimens adsorbed water from the atmosphere rather quickly. To determine the rates of weight gain, one eroded sample of each composition was aged in laboratory air for various times to 2.4×10^5 s. Weight gains were significant relative to weight losses from erosion testing (Fig. 1). Differential thermal analysis (DTA) measurements in air (Al_2O_3 standard; heating rate = 8.3×10^{-2} K/s) made with a Harrop DT726 confirmed presence of substantial adsorbed volatiles, which evolved below ≈150 °C (Fig. 2).

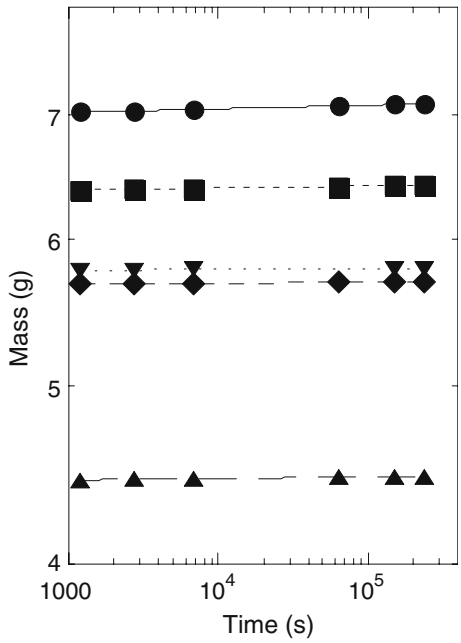

Fig. 1 Weight-gain data due to adsorption for specimens eroded at 30° and 50 m/s: A (●), B (▲), C (◆), D (■), and E (▼)

Table 1 Compositions of geopolymer samples

Specimen	Additive 1	Additive 2	Sand/slag	Alkali activator
A	Slag 800 g	Sand 2.4 kg	3:1	660 g
B	Slag + flyash 800 g	Sand 2.4 kg	3:1	525.5 g
C	Slag + flyash 810 g	Sand 2.4 kg	3:1	505.5 g
D	Slag + flyash + clay 800 g	Sand 1.2 kg	3:2	508 g
E	Slag + flyash 24 kg	Sand + rock 62 kg	≈3:2	13.4 kg

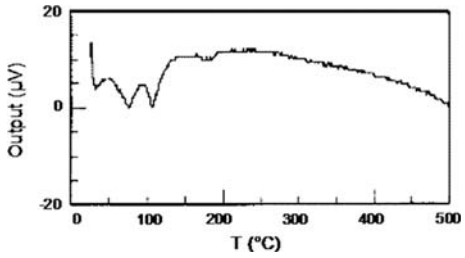

Fig. 2 DTA data from Specimen D heated in air at 8.3×10^{-2} K/s

To minimize possible problems with the weight-loss measurements due to environmental effects such as adsorption of water, experiments to determine individual ER values were completed within one day. Following each run, specimens were removed, brushed, cleaned by an air blast, and weighed. Each cycle of specimen removal from the eroder through weighing took 14 ± 2 min. It is estimated that the average weight-loss measurement was accurate to ±5%. Uncertainties arose due to incomplete cleaning of the surfaces and slight adsorption of water. For single-impact tests, only 5 g of Al_2O_3 abrasive were fed into the eroder so that only a few impact sites overlapped.

SEM was used to correlate damage morphology of the eroded surfaces with the weight-loss measurements. Steady-state and single-impact damage sites were examined.

Results and discussion

The geopolymer specimens contained significant porosity. Average densities were 2.0–2.2 g/cm^3, which is typical for such geopolymers [27, 28]. Crushing strength correlated with density for the three most-similar specimens, B–D, all of which contained slag, flyash, and sand. Strengths were lower for Specimen A, which did not contain flyash, and Specimen E, which contained the large basalt inclusions (Table 2). One presumes that the sharp edges of the basalt created stress concentrations, which led to reduced strength.

The microstructures consisted of aggregates of various sizes and shapes bonded by a largely amorphous matrix.

Table 2 Specimen designation and type, density, compressive strength after aging for 28 d, and ER for 90° impact at 50 m/s

Specimen	Additives	Density (g/cm^3)	Strength (MPa)	ER_{90} (mg/g)
A	Slag, sand	2.09	41	49.6
B	Flyash, slag, sand	2.03	40	11.3
C	Flyash, slag, sand	2.22	58	7.6
D	Flyash, slag, clay, sand	2.08	44	8.8
E	Flyash, slag, sand, basalt	2.05	35	6.9

The aggregates were remnants of sand or slag particles. The aggregates were largest in Specimen A, the one that did not contain flyash. The basalt inclusions in Specimen E were as large as ≈15 mm in maximum dimension (Fig. 3). Microcracks, especially along matrix/aggregate interfaces, were prevalent in all specimens (Fig. 4).

Representative data for specimen weight loss versus dose of impacting particles are shown in Fig. 5. ER was defined as the slope of the linear least-squares fit to the data for weight lost per weight of particles striking the surface (Fig. 5b). The fits did not in general extrapolate through the origin, which is common for brittle materials that have not been polished. Adsorbed water may also have affected the first set of weight-loss measurements. ER was generally highest for specimens tested at 90° and lowest at 30°. The data were consistent for each specimen and it is estimated that ER values were accurate to ±10%. However, duplicates of Specimen D tested at 90° revealed significant sample-to-sample variation in erosion rate, ≈20% [23]. The scatter in the data for duplicate specimens was probably more attributable to differences between samples rather than difficulty to making reproducible measurements. The consistency of erosion-rate measurements in this apparatus has been excellent, typically plus or minus a few percent [23].

Erosion rates ER for brittle materials should be highest at 90° and lowest at glancing incidence [25, 28–35]. The data for 100 m/s followed the expected trend well, those at 50 and 70 m/s less well (Fig. 6). At 50 m/s impact, ER was almost independent of angle of impact. This trend with velocity and angle has been related to presence of aggregates and microcracks in each sample and to the effects of removal of aggregates on a comparatively large scale [23]. Rather than removing material through a series of elastic-plastic interactions that induce radial and lateral cracks, relatively large pieces were lifted from the surface. The unexpected results for erosion rate versus angle and velocity have been ascribed to microstructural effects that affect erosion at oblique impact; erosion for normal incidence is, and has been shown to be [23], typical of complex brittle solids.

It has been observed that erosion rates in brittle materials impacted at oblique incidence are inevitably higher than would be predicted from consideration of only the normal component of velocity and formation of lateral cracks [24, 34, 35]. Contributions from Mode II or Mode III loading are thought to be likely [35]. In addition, as we noted in our previous study of erosion of a specific geopolymer [23], simple geometric arguments indicate that radial cracks may also contribute to material loss for oblique impact into roughened surfaces. Radial cracks are, for example, thought to contribute significantly to material loss in porous ceramics [36, 37]. As we speculated in Ref. 23,

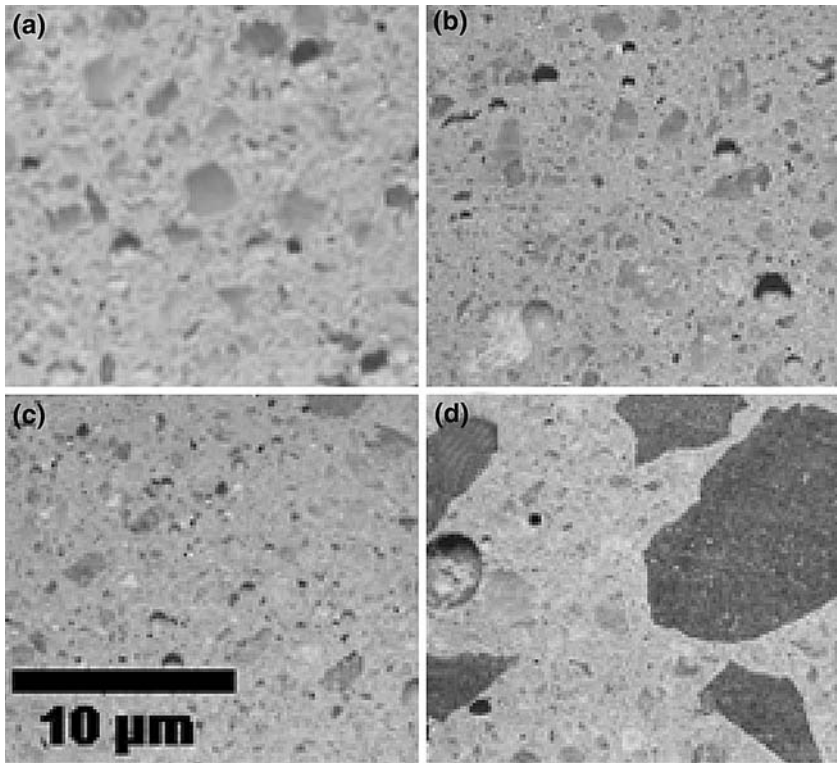

Fig. 3 Optical photomicrographs of representative microstructures of (**a**) Specimen A, (**b**) Specimen B, (**c**) Specimen D, and (**d**) Specimen E; B and C were nearly identical and so only B appears

the relatively high erosion rates for impact at 30° are probably caused by effects of Modes II and III loading and the ease with which aggregates could be removed.

Erosion rate versus velocity for each angle can be inferred from Fig. 6. Models of erosion of brittle materials predict that *for normal impact* ER $\propto V^n$, where n ranges from 2.0 to 3.4 [28–30]. Values of n for geopolymers Specimens B–E impacted at 90° ranged from 2.3 ± 0.3 to 2.7 ± 0.3; the error bars reflect estimates of uncertainty inherent in making the measurements and the quality of the statistical fit to the data. These values are close to the values of 2.3–2.4 predicted by the models of Ritter et al. [31] and Weiderhorn and coworkers [29–30]. SEM revealed, however, that the erodent traveling 100 m/s fractured substantially upon impact. Such fracturing was not evident for erodent velocities of 50 and 70 m/s (Fig. 7). Fracturing of erodent will dissipate energy, and thus lower erosion rates. The weight-loss data at 100 m/s were thus lower than they should have been, and the calculated values of n were in fact lower than they should have been. We cannot, however, estimate the extents to which the n values were reduced.

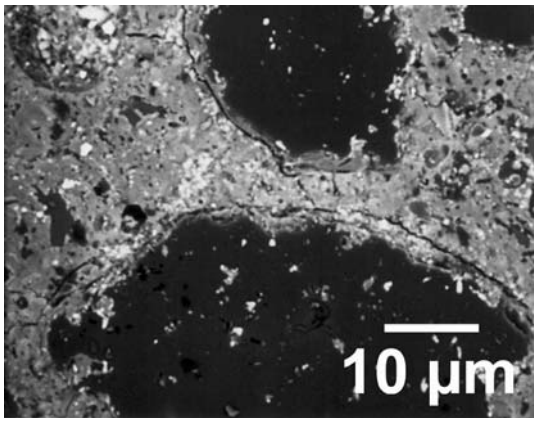

Fig. 4 SEM photomicrograph of Specimen D in which microcracks are evident at interface between geopolymer matrix and sand inclusions; this region was among the most-severely microcracked

The data obtained were far from ideal. Weight-loss measurements were rendered approximate because of water adsorption, high-velocity weight losses were reduced in magnitude because of erodent fracture, and the microstructures of the geopolymers were nonuniform and contained voids and cracks. These deviations from ideality argue for caution when analyzing the data. Most important to this inquiry are the observations that (1) Specimen A, the one without flyash, eroded much more rapidly than did the others (in fact it eroded so rapidly at 50 m/s that we did not even test it at 70 and 100 m/s) and (2) Specimen E, which contained the large basalt inclusions, eroded approximately as rapidly as did specimens B–D.

Material loss is a sequential event for ideal brittle materials impacted at near-normal incidence by sharp erodents: (1) Indentation creates an elastic-plastic zone

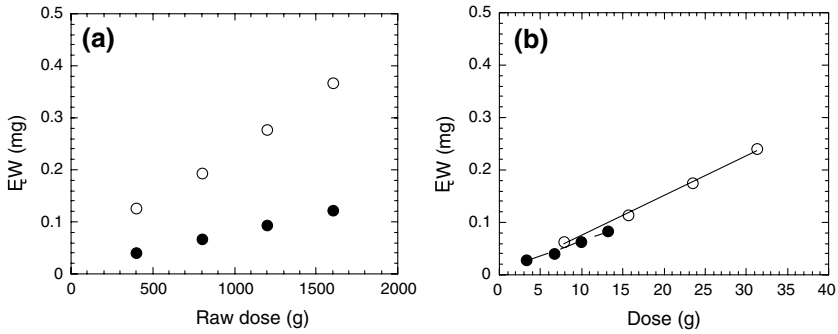

Fig. 5 Weight loss versus erodent dose for geopolymer Specimen C eroded at 50 m/s impacted at 90° (○) and 30° (●): (**a**) raw dose into eroder and (**b**) dose actually impacting samples; ER values defined as slope of lines in (b)

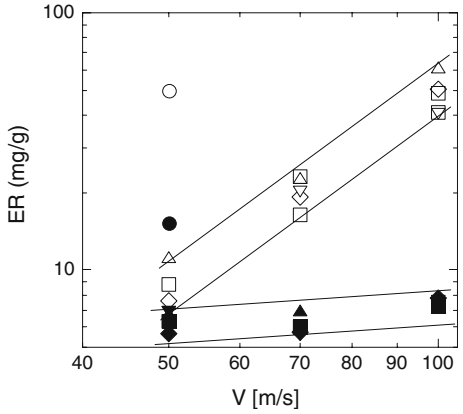

Fig. 6 ER versus velocity for geopolymer specimens eroded at 90° (open symbols) and 30° (filled symbols): A = circles, B = triangles, C = diamonds, D = squares, and E = inverted triangles

beneath the impacting particle. (2) Radial cracks roughly perpendicular to the specimen surface form below the elastic-plastic zone; these cracks are induced by Mode I loading. (3) As the erodent particle recoils, a resulting tensile stress state induces formation of lateral cracks approximately parallel to the surface. (4) The lateral cracks propagate to the surface and chips are removed [25, 28–33]. The SEM observations were generally consistent with erosion of classically brittle ceramics. The steady-state erosion surfaces were irregular and overlapping brittle cleavage fractures were evident (Fig. 8). The single-impact sites were also characteristic of erosion of a brittle solid. Two basic types of events were observed. Some of the impacts evinced material removal, along with formation of many comparatively small cracks (Fig. 9a). Other impacts were more-characteristic of erosion of a classical brittle solid [34]: indenting, radial-crack formation, and propagation of lateral cracks (Fig. 9b).

Although the responses to impact of the geopolymers were more complex than that of a classical brittle solid such as glass [35] or silicon single crystals [34], they were dominated by brittle fracture and models of erosive response should be applicable for impact at 90°. The question as to effect of geopolymer composition on erosion rate can be addressed best by dividing the five specimens into three categories: based on slag (Specimen A), based on slag + flyash (Specimens B–D), and based on slag + flyash + large basalt inclusions (Specimen E).

The rapid erosion of Specimen A clearly indicates a benefit from adding flyash to the geopolymer mix. The exact mechanisms by which flyash imparts this benefit are under investigation. Possibilities include improved adhesion to retained particles in the microstructure, increased resistance to erosion of flyash-based particles compared with those from other precursors, and fundamental differences in reaction pathways leading to differences in size and shape of retained precursor particles.

For specimens with flyash (B, C, and D), erosion rate correlated with density and strength. The denser, stronger specimens were generally more resistant to erosion. These results are as one would expect for a brittle material in the absence of extraneous influences.

Specimen E is an example of the type of composite for which erosion has been studied previously: discrete phases for which individual impact sites are small relative to the

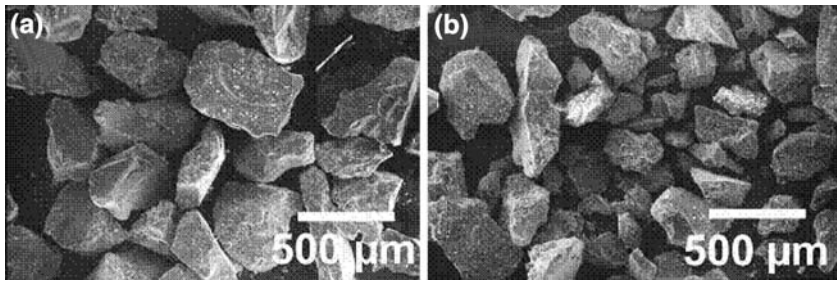

Fig. 7 SEM photomicrographs of Al_2O_3 erodent after testing at (**a**) 50 m/s and (**b**) 100 m/s; small debris is evident in both images and significant fracturing of the spent erodent after impacting at 100 m/s is clear

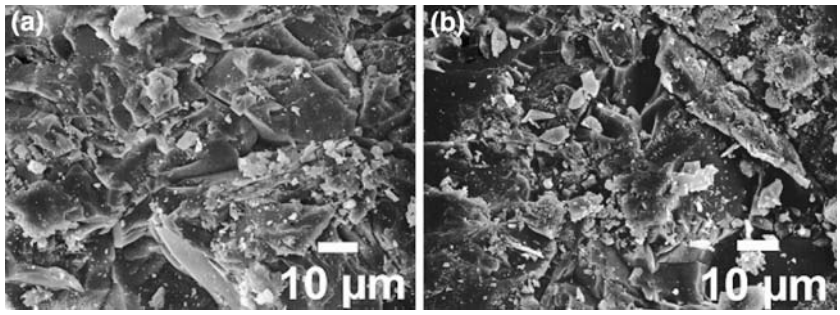

Fig. 8 SEM photomicrographs of steady-state erosion surfaces of Specimen B eroded at 50 m/s: (**a**) at 90°a and (**b**) at 30°; the surfaces evince similar features

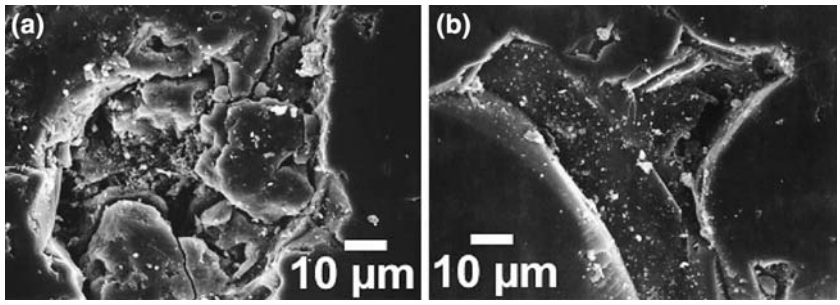

Fig. 9 SEM photomicrographs of single-impact damage sites in geopolymers impacted at 70 m/s and 90°: (**a**) Specimen A and (**b**) Specimen D

sizes of the phases [38, 39]. For such composites, weight loss W from erosion is

$$1/W = m_1/W_1 + m_2/W_2, \quad (1)$$

where m_1 is the mass fraction of Phase 1 and W_1 is the weight loss of Phase 1 and the subscript 2 refers to Phase 2. This so-called inverse rule of mixtures [39] accounts for density. The density of Specimen E was 2.05 g/cm^3 and that of the basalt should have been ≈2.9 g/cm^3 [40]. The density of the geopolymer surrounding the basalt was therefore ≈1.9 g/cm^3, slightly less than that of the other specimens. Application of Eq. 1 to the data in Fig. 6 and Table 2 implies that the basalt was more erosion resistant than the geopolymers *on a volume basis*. Visual inspection confirmed this hypothesis: in heavily eroded specimens, the basalt protruded above the surrounding geopolymer. An obvious way to improve erosion resistance of this type of composite would be to increase the fraction of large erosion-resistant particles that are themselves large compared with the erodent particles.

The models for erosion of brittle materials provide further guidance as to how the resistance of slag-flyash geopolymers might perhaps be further improved. Erosion rates are, in general, related to the lengths of lateral and radial cracks that form. For impact pressure P, the lateral cracks that form have length c_L, where

$$c_L = A\left[F(E/H)^{3/4}/K_c H^{1/4}\right]^{1/2} P^{5/8}, \quad (2)$$

where A is a constant, F is a geometric factor, E is the target elastic modulus, H is the target hardness, and K_c is the critical stress-intensity factor of the target [33]. For impact pressure P, the radial cracks that form have length c_R, where

$$c_R = \left[F * (E/H)^{1/2}/K_c H^{1/4}\right]^{2/3} P^{2/3}, \quad (3)$$

where F* is a geometric factor and the other terms are as defined in Eq. 2 [32]. It would seem that increasing K_c would provide the greatest benefit. Geopolymer composites with improved fracture toughness [41, 42] have been produced and they may prove to be more erosion resistant than did these unreinforced geopolymers. Mechanical properties of geopolymers, and how to improve them, is a focus of current efforts [43] and it is likely that geopolymers, probably in composite form, that are more resistant to erosion will be produced soon.

Conclusion

Geopolymers derived from various combinations of granulated blast-furnace slag, Class C flyash, clay, sand, and basalt were tested for resistance to solid-particle erosion. The geopolymer that did not contain flyash eroded most rapidly. Flyash promoted dissolution of the slag and sand aggregates, but the mechanism by which its presence improved erosion resistance has yet to be identified. The geopolymers that contained flyash exhibited similar erosion rates, with resistance to erosion improving with increased density and strength of the specimens. Addition of basalt had only a minor effect on erosion rate, as

measured by weight loss, but a beneficial effect when measured by volume loss. For all specimens, erosion proceeded by propagation of brittle cracks. Presence of comparatively large particles and cracks in all of the geopolymers was concluded to accelerate erosion for impact at 30°.

Acknowledgements The work at Argonne National Laboratory was supported by the U.S. Department of Energy, under Contract W-31–109-Eng-38. The work at The University of Melbourne was partially supported by a contract from the Asian Office of Aerospace Research and Development. We thank Dr. Robert Erck for assistance with some of the photographs and Dr. Nan Chen for assistance with some of the experiments.

References

1. Davidovits J, Proceedings of PACTEC '79, Society of plastic engineers, Brookfield, CT, 1979, p 151
2. Davidovits J (1991) J Therm Anal 37:1633
3. Davidovits J, In: Krivenko PV (ed) Proceedings of the 1st international conference on alkaline cements and concretes, VI-POL Stock Co., Ukraine, 1994, p 131
4. Gordon M, Bell J, Kriven WM (2005) Ceram Trans 165:95
5. Campbell KM, EL-Korchi T, Gress D, Bishop P (1987) Environ Prog 6:99
6. Van Jaarsveld JGS, Van Deventer JSJ, Lorenzen L (1998) Metall Mater Trans B 29:283
7. Xu H, Van Deventer JSJ (2000) Int J Miner Proc 59:247
8. Phair JW, Van Deventer JSJ, Smith JD (2000) Ind Eng Chem Res 39:2925
9. Van Jaarsveld JGS, Van Deventer JSJ, Schwartzmann A (1999) Miner Eng 12:75
10. Xu H, Van Deventer JSJ, Lukey GC (2001) Ind Eng Chem Res 40:3749
11. Van Jaarsveld JGS, Van Deventer JSJ, Lukey GC (2002) Chem Eng J 89:63
12. Yip CK, Lukey GC, Van Deventer JSJ (2003) Ceram Trans 153:187
13. Duxson P, Lukey GC, Van Deventer JSJ, Mallicoat SW, Kriven WM (2005) Ceram Trans 165:95
14. Fwa TF, Low EW (1990) Cem Concrete Aggreg 12:101
15. Momber A, Kovacevic R (1994) Wear 177:55
16. Singh D, Wagh AS, Cunnane J Mayberry J (1997) Environ Sci Health, A32:527
17. Wagh AS, Strain R, Jeong SY, Reed D, Krause T, Singh D (1999) J Nucl Mater 265:265
18. Lyon RE, Balaguru PN, Foden A, Sorathia U, Davidovits J, Davidovics M (1998) Fire Mater 21:67
19. Fletcher RA, Mackenzie KJD, Nicholson CL, Shimade S (2005) J Euro Ceram Soc 25:1471
20. Goretta KC, Burdt ML, Cuber MM, Perry LA, Singh D, Wagh AS, Routbort JL (1999) Wear 224:106
21. Goretta KC, Singh D, Tlustochowicz M, Cuber MM, Burdt ML, Jeong SY, Smith TL, Wagh AS, Routbort JL (1999) Mater Res Soc Symp Proc 556:1253
22. Goretta KC, Chen N, Routbort JL, Lukey GC, Van Deventer JSJ, Van Jaarsveld JGS, Lloyd RR, Geopolymers 2002—CD Proceedings In: Lukey GC (ed) Siloxo, Melbourne, 2003
23. Goretta KC, Chen N, Gutierrez-Mora F, Routbort JL, Lukey GC, Van Deventer JSJ (2004) Wear 256:714
24. Australian Standard AS 1012.9, Methods for testing concrete (1986)
25. Routbort JL, Scattergood RO (1992) Key Eng Mater 71:23
26. Hos JP, McCormick PG, Byrne LT (2002) J Mater Sci 37:2311
27. Wang JW, Cheng TW, Proceedings of the 7th International Symposium on East Asian Resources Recycling Technology, In: Tsai M-S (ed) Tainan, Taiwan, 2003, http://www.ntut.edu.tw/~twcheng/S4R104.pdf, as on 12 July 2005
28. Evans AG, Gulden ME, Rosenblatt M (1978) Proc R Soc London Ser A 361:343
29. Wiederhorn SM, Lawn BR (1979) J Am Ceram Soc 62:66
30. Wiederhorn SM, Hockey BJ (1980) J Mater Sci 18:766
31. Ritter JE, Strzepa P, Jakus K, Rosenfeld L, Buckman KJ (1984) J Am Ceram Soc 67:769
32. Lawn BR, Evans AG, Marshall DB (1980) J Am Ceram Soc 63:574
33. Marshall DB, Lawn BR, Evans AG (1982) J Am Ceram Soc 65:561
34. Routbort JL, Scattergood RO, Kay EW (1980) J Am Ceram Soc 63:635
35. Srinivasan S, Scattergood RO (1987) J Mater Sci 22:3463
36. Martínez-Fernández J., De Arellano-López AR, Varela-Feria FM, Orlova TS, Goretta KC, Gutierrez-Mora F, Chen N, Routbort JL (2003) J Euro Ceram Soc 24:861
37. Goretta KC, Gutierrez-Mora F, Chen N, Routbort JL, Orlova TS, Smirnov BI, De Arellano-López AR (2003) Wear 256:233
38. Anand K, Morrison C, Scattergood RO, Conrad H, Routbort JL, Warren R (1986) Inst Phys Ser No 75:949
39. Hovis SK, Talia JE, Scattergood RO (1986) Wear 108:139
40. PINET P, The Planet Oceanus, http://www.marine.usm.edu/mar151/MAR_151_Chap_2.html, as on 20 July 2005
41. Hammell J, Balaguru P, Lyon R (1998) SAMPE Proc 43:1600
42. Papakonstantinou CG, Balaguru P, Lyon RE (2001) Comp Part B 32:637
43. Duxson P, Provis JL, Lukey GC, Mallicoat SW, Kriven WM, Van Deventer JSJ (2007) Coll Surf A 292:8